Time-dependent Monte Carlo calculations of recoil-in-vacuum g-factor data for ^{122,126,130,132}Te

X. Chen, D. G. Sarantites, W. Reviol, and J. Snyder

Phys. Rev. C **87**, 044305 — Published 4 April 2013

DOI: 10.1103/PhysRevC.87.044305

Time-dependent Monte-Carlo calculations of recoil-in-vacuum g-factor data for ^{122,126,130,132}Te

X. Chen[1], D. G. Sarantites[1], W. Reviol[1], and J. Snyder[2]

[1]*Department of Chemistry, Washington University, St. Louis, MO. 63130*

[2]*Department of Physics, Washington University, St. Louis, MO 63130*

(Dated: March 5, 2013)

Abstract

A method for extracting nuclear g factors from the attenuation coefficients G_k (k = 2 ,4) of γ-ray angular distributions or particle-γ angular correlations measured with the recoil-in-vacuum (RIV) technique is presented. The method uses time-dependent Monte-Carlo simulations for G_k, as a function of the g factor for given nuclear lifetime. It is based on atomic-structure calculations from first principles using the GRASP2K code by Jönsson *et al.* The simulations are compared with results of RIV measurements for the first excited states (2_1^+) in ^{122,126,130,132}Te. The choice of the electronic configurations and the effect of the charge-state distributions on G_k are discussed. New 2_1^+ g-factor values are obtained. These are compared with nuclear-model calculations.

PACS numbers: 27.10.Ky, 31.30.Gs, 31.15.A-,23.20.En

I. INTRODUCTION

The recoil-in-vacuum (RIV) technique [1] utilizing the magnetic hyperfine interaction between the nucleus and its orbital electrons was first introduced in the 1970's to measure g factors of excited nuclear states with ps lifetimes. At that time RIV studies focused on light elements [2–4] and a few medium-mass nuclei [5] had been studied as well. The technique is quite straightforward. It is based on the measured attenuation of the γ-ray angular distribution (AD) or particle-γ angular correlation (AC) due to the magnetic hyperfine interaction. Typically, in a Coulomb-excitation experiment the AC attenuation is determined from a thin-target measurement (perturbation due to recoiling of the γ-ray emitter in vacuum) and a measurement with a thin target backed by a thick non-magnetic layer (no perturbation) by dividing the respective AC coefficients. The corresponding attenuation coefficients are denoted $G_k(k = 2, 4)$. The fact that the technique was seldom used in the past was probably due to the complexity of the electronic configurations of the recoiling ions and the associated difficulty in calibrating the magnetic hyperfine interaction. In 2005, Stone *et al.* [6] reported the first result of a RIV analysis of a radioactive-ion beam experiment and the g factor of the first excited state , 2_1^+, of ^{132}Te was determined. The experimental success and the recent progress in atomic theory (see below) indicate that the RIV technique has been revived and is a promising method to measure g factors. This is of particular interest for studies of exotic nuclei, which can be accessed now by projectile Coulomb excitation.

For g-factor measurements of short-lived states, the transient field (TF) technique [7] has been widely used. It has the advantage of being able to measure both the magnitude and sign of the g factor. However, this technique requires using a thick target with a ferromagnetic layer as backing and an external magnetic field. For projectile g-factor measurements, this condition causes a problem: the thick target may induce a large radioactive background. On the other hand, with a thin target as used for a RIV experiment the background is comparatively small. Moreover, the AD or AC attenuation in RIV experiments can be measured utilizing all the detectors in a near 4π detector array, whereas the optimal precession sensitivity for the TF technique is achieved only for detectors in the plane perpendicular to the direction of the external magnetic field [6]. Thus, the RIV technique has the potential of performing g-factor measurements with higher statistical accuracy than the TF technique does. However, the RIV technique is insensitive to the sign of the g factor and relies on

systematics and/or a measurement of the sign by the TF method.

Since the pioneering measurement of Stone *et al.* [6], many efforts have been made to calibrate and model the RIV hyperfine interaction. The interaction was usually described by the strength of the hyperfine magnetic field at the nucleus where the field was approximated with an empirical model. This seemed to be the best procedure, since the relation between the electronic configurations and the field is complicated. Specifically, a static model was used where G_k was calculated under the assumption that the electronic-state lifetimes are much longer than the nuclear lifetime. In 2007, Stuchbery and Stone [8] reexamined the calibration of the RIV interaction for previously published RIV data on Te ions [6] and reevaluated the g factor for 2_1^+ state of ^{132}Te. They introduced a modified static model, using an average electronic-state lifetime and a time range for the multi-step decay to the ground state as free parameters, that improved the fit to the data (cf. Sec. II B).

A recent experimental development, using a recoil-distance device (plunger), is the measurement of differential attenuation coefficients $G_k(d)$ where d represents the target-to-stopper distance [9]. This indicates once more the increasing interest in the RIV technique.

With the availability of an advanced atomic theory for many-electron ions [10], it is possible to calculate the hyperfine interaction from first principles rather than relying on an estimated hyperfine-field strength. The paper by Stone *et al.* [11] may be viewed as a pioneering contribution in this sense. The calculations of G_k in Ref. [11] have been made with the original static model based on the assumption of long-lived electronic states. However, as shown in Ref. [12], many relevant atomic states have lifetimes comparable to or shorter than the nuclear lifetimes. In Ref. [11], it is pointed out that transitions between the electronic states may be important in G_k calculations as the hyperfine interaction may change when the highly excited, short-lived electronic states decay within a time period comparable with the nuclear lifetime. Also, it is suggested in Ref. [8] that the RIV data for certain Te isotopes can be fitted better with the modified static model if in the G_k calculations several atomic transitions were allowed on a timescale compatible with the nuclear lifetime.

We have taken an approach different from the static model. Here the contributions from a large number of electronic states are taken into account according to their lifetimes and partial widths. The approach is still in the spirit of Ref. [11] in that the hyperfine interaction is calculated from first principles. The approach is applied to the data from the projectile

Coulomb-excitation studies of ^{122,126,130,132}Te, for which G_k values are reported in Ref. [8]. In these cases the present approach is validated and new values for the g factors are obtained.

The set of stable and neutron-rich Te isotopes is attractive both from a theoretical and an experimental point of view. First, these isotopes are located near the doubly-magic ^{132}Sn, a region important for the development of nuclear theory, and the measured g factors help to test various theoretical models. Second, the RIV data for ^{122,126,130,132}Te represent a prototype g-factor measurement for new studies with other radioactive-ion beams, where the data could be analyzed with the present approach.

II. RIV TECHNIQUE

A. The Principle

The basics of the RIV technique are described in Refs. [1, 6] and are briefly summarized hereafter. The excited nucleus, as obtained from e.g. Coulomb excitation, recoils with a few percent of the speed of light ($\beta \sim 0.03$ to 0.1) where the atom is ionized. The hyperfine interaction couples the atomic spin, $\mathbf{J}$, to the nuclear spin, $\mathbf{I}$, making them precess about the resultant vector $\mathbf{F} = \mathbf{I} + \mathbf{J}$. Thus the initial alignment of the nuclear spin, formed by Coulomb excitation, will be reduced. The G_k coefficients introduced in Sec. I are measured as the ratios $A_k^{(a)}/A_k^{(u)}$, the attenuated AC coefficients divided by the unattenuated ones. The G_k coefficients are functions of the mean lifetime of the nuclear state, τ, and the precession frequency, $\omega_{FF'}$, which is proportional to the g factor and where F and F' represent initial and final couplings.

Following Goldring's presentation [1], the time dependent attenuation coefficients $G_k(t)$ for a given pair of quantum numbers I and J can be expressed as

$$G_k(t) = 1 - 2 \times \sum_{F>F'} \frac{(2F+1)\,(2F'+1)}{(2J+1)} \left\{ \begin{array}{ccc} F & F' & k \\ I & I & J \end{array} \right\}^2 \left[1 - \cos\left(\omega_{FF'} t\right)\right], \qquad (1)$$

where $\omega_{FF'}$ is related to the hyperfine interaction constant A and the g factor via the expressions

$$\omega_{FF'} = \frac{A}{\hbar} \cdot \left[F(F+1) - F'(F'+1)\right]/2, \qquad (2)$$

$$A = g\frac{B\mu_{_N}}{J}, \tag{3}$$

where μ_N and B denote the nuclear magneton and the magnetic hyperfine field at the nucleus, respectively.

The time-integral attenuation coefficients $G_k(\infty)$ that refer to the static model are obtained by the integration

$$G_k(\infty) = \frac{1}{\tau}\int_0^\infty e^{-t/\tau} G_k(t) dt, \tag{4}$$

and are given in Ref. [6] as

$$G_k\left(\infty\right) = \sum_{FF'} \frac{\left(2F+1\right)\left(2F'+1\right)}{\left(2J+1\right)} \left\{ \begin{array}{ccc} F & F' & k \\ I & I & J \end{array} \right\}^2 \frac{1}{\left(\omega_{FF'}\tau\right)^2+1}. \tag{5}$$

The various implementations of the static model and the present approach differ in the evaluation of $\omega_{FF'}$. In the approach of Ref. [8] the expression for A according to Eq. (3) is used and the field B is treated as a parameter. In the approach taken in Ref. [11] for the static model, and in the time-dependent approach of the present work, the hyperfine constant A of Eq. (2) is evaluated, according to Ref. [10], as

$$A = g \cdot A_{int}, \quad A_{int}=\frac{\left\langle \Gamma_J J \left\| T^{(1)} \right\| \Gamma_J J \right\rangle}{\left[J(J+1)(2J+1)\right]^{1/2}}, \tag{6}$$

where $\left\langle \Gamma_J J \left\| T^{(1)} \right\| \Gamma_J J \right\rangle$ is the reduced matrix element for the magnetic-dipole operator in the atomic-wavefunction space. This space is defined by J, and a set of quantum numbers, Γ_J, which represent the electron configuration for a given J. The $T^{(1)}$ represents the magnetic-dipole tensor operator, the explicit expression of which is given by Eq. (8.50) in Ref. [10].

In the static model the electron configuration is assumed not to change during the nuclear lifetime. Since $\omega_{FF'}$ is proportional to the g factor and the coefficients $G_k(\infty)$ are explicit functions of $\omega_{FF'}\tau$ according to Eq. (5), the $G_k\left(\infty\right)$ factors can be expressed as functions of the product $g\tau$. This is done in the literature where the static model is used.

B. Uses of the static model

In the experiments of Ref. [6], G_k coefficients were extracted for the 2_1^+ states of the "calibration" isotopes ^{122,126,130}Te. They were then fitted with the static model. The J-state distribution and the magnitude of the hyperfine interaction were adjusted such that the $G_k(g\tau)$ functions fit the G_k values for ^{122,126,130}Te. From these functions and the G_k values for ^{132}Te the $g\tau$ value for the 2_1^+ state of ^{132}Te was determined. With the known lifetime for this state [13], a g factor 0.35(5) was obtained, where the positive sign was based on systematics. Recently, a revised g-factor value of 0.46(5) has been reported, as a consequence of a correction of the nuclear lifetime [14].

As mentioned in Sec. I, the results for the Te isotopes [6] were reexamined in Ref. [8]. Gaussian shapes were assumed for both the J-state and B-field distributions, and the corresponding centroids and widths were discussed. To improve the fits to the data, atomic fluctuations were allowed in the modified static model. Here the parameters τ_E and τ_A were introduced, with τ_E determining how often the ensemble of the many-electron ions tries to make a transition and τ_A determining whether the atom is allowed to make the transition. The fact that the RIV data for the Te isotopes with longer nuclear lifetimes can be fitted better with the modified static model indicates that the atomic transitions during the nuclear lifetime may play an important role in the calculations of the coefficients G_k. This seems especially true for the nuclear states with longer lifetimes, where the G_k may approach the so-called hard-core value (see Sec. I of Ref. [1]).

It should be reemphasized that in the static model all relevant electronic lifetimes are assumed to be much longer than τ. This is not always true, many electronic states may have lifetimes comparable to or shorter than τ. Some of the short-lived electronic states may contribute strongly to the hyperfine interaction.

In Ref. [11], in order to determine the coefficients G_k, the hyperfine interaction is calculated with the advanced atomic-structure package, GRASP2K, by Jönsson *et al.* [15]. This package uses multi-configuration Dirac-Hartree-Fock theory [10] for many-electron ions to calculate atomic-level wavefunctions, level energies, and transition probabilities among other quantities. The results show great promise in that such calculations could provide parameter free, "a-priori" analyses of RIV experiments. Notably, the authors in Ref. [11] question the assumption that the hyperfine interaction is "static" during the nuclear lifetime, they state

that the original model sometimes gives poor agreement with experiment, and that allowing for decay improves the agreement.

C. Time-dependent Monte-Carlo simulations for the RIV g factors

Following Ref. [11], we are using GRASP2K to calculate the properties of the excited atomic states. We have devised a procedure where Monte-Carlo simulations based on the time dependent attenuation formula of Eq. (1) are carried out. To estimate the G_k contribution from each atomic state to the average G_k more precisely than previous approaches did, we take into account transitions between atomic states and their associated state lifetimes. That is, level energies, parameters A_{int} (according to Eq. (6)), and transition probabilities of the states are calculated.

The procedure to determine the average value of G_k includes five steps: (1) The distribution of the charge states w_Q in the recoiling ion with nuclear charge Z is calculated with the code CHARGE [16]. (2) For each charge state Q of the stripped ion, the appropriate atomic states are chosen by specifying a reference electronic configuration and the number of excitations. The reference configuration represents the lowest energy manifold of atomic states determined in the j-j coupling scheme with $Z - Q$ electrons. The number of excitations, n_E, has to be specified which is equivalent to the number of electrons to be excited. For example, if $n_E = n$, it means that electronic configurations with non-electron excitation (ground state configuration), one-electron excitation, and up to n-electron excitation are included in the atomic structure calculation. The corresponding level energies and A_{int} parameters, are calculated. (3) The transition probabilities and subsequently the lifetimes τ_{a_i} for all atomic states are calculated. The lifetime of an atomic state is the inverse of the sum of the transition probabilities from this level to all lower-lying levels [10]. (4) A Monte-Carlo simulation is performed in order to get $G_{k,Q}(\tau, g)$ as a function of the g factor for a given value τ, and for each charge state. (5) The final attenuation coefficient $G_k(\tau, g)$ is computed as a weighted average over all the charge states $G_{k,Q}(\tau, g)$.

In step (3), only $E1$ transitions are allowed; $M1$ and higher-multipole transitions are considered as too slow and are omitted. Here a Python code is used to calculate the lifetimes and store these in a database, together with the transition probabilities between every pair of atomic states of opposite parity. Notably, the Monte-Carlo simulation in step (4) is

performed with another Python code.

The time sequence on which the simulation of an event is based is illustrated in Fig. 1. The corresponding expressions for choosing the appropriate hyperfine interaction for each event are presented below. The sequence of steps in the simulation of an event is the following: (A) A nuclear survival time, t_n, is chosen randomly, weighted according to the decay function $e^{-t_n/\tau}$. (B) To start an event, an atomic state dubbed the "first" state is randomly chosen from a list of states which were generated in step (2) above. The list of atomic states for a given charge state may include up to 4,000 entries. These originate from a significantly smaller number of electronic configurations. The weight given to a state with spin J is taken as $(2J+1)$. (C) Depending on the mean lifetime τ_{a_1} of the "first" atomic state, a value for its survival time, t_{a_1}, is chosen randomly that is weighted according to the exponential decay $e^{-t_{a_1}/\tau_{a_1}}$. The hyperfine-interaction time, t_{int_1}, is determined by the smaller of the two times t_n and t_{a_1}. The hyperfine interaction parameter for this state is denoted A_{int_1}, and the corresponding time-dependent attenuation coefficient $G_k(t_{int_1})$, is calculated from Eq. (1). (D) The following decision is made. If the chosen interaction time is found to be longer than t_n ($t_n < t_{a_1}$), then the nuclear state has decayed before the atomic state and the simulation of the event is finished. Otherwise, a "second" atomic state will be chosen randomly from the possible states below the "first" state, based on the decay probability to the possible atomic states below. (E) The two previous steps, (C) and (D), are repeated as many times as necessary, with the parameters A_{int_i} and t_{int_i} of the i^{th} atomic state, until the "last" atomic state is reached. Note that t_{int_i} is equal to the survival time t_{a_i}, if $t_{a_i} \neq t_{a_{last}}$. The condition

$$t_{a_{last}} > t_n - \sum_{i=1}^{last-1} t_{a_i}, \tag{7}$$

determines the interaction time for the last state with $t_{a_{last}}$, and the interaction time becomes

$$t_{int_{last}} = t_n - \sum_{i=1}^{last-1} t_{a_i}. \tag{8}$$

The coefficient for an event, $G_k^s(\tau, g)$, where s denotes the number of the event in the simulation, is the product of coefficients $G_k(t_{int_i})$

$$G_k^s(\tau, g) = \prod_{i=1}^{last} G_k(t_{int_i}). \tag{9}$$

The coefficient $G_{k,Q}(\tau, g)$ for each charge state is the average of the $G_k^s(\tau, g)$ values of all events m in the simulation

$$G_{k,Q}(\tau, g) = \frac{\sum_{s=1}^{m} G_k^s(\tau, g)}{m}. \tag{10}$$

The final $G_k(\tau, g)$ values are calculated as weighted averages over all charge states, i.e.,

$$G_k(\tau, g) = \sum_{Q=Q_{\min}}^{Q=Q_{\max}} w_Q G_{k,Q}(\tau, g), \text{ with } \sum_{Q=Q_{\min}}^{Q=Q_{\max}} w_Q = 1.$$

III. TESTS AND RESULTS

A. Tests of the simulation procedure

The RIV experiment for ^{122}Te [6] is chosen for testing the simulation procedure. Compared to other Te isotopes, the previous measurements for ^{122}Te gave consistent g-factor values for the 2_1^+ state. The G_k values for the 2_1^+ state of ^{122}Te is closer to the hard-core value than those of the other Te isotopes; this is due to the longer ^{122}Te nuclear lifetime. The experimental details and measured G_k coefficients for four Te isotopes (^{122,126,130,132}Te) are listed in Table I. The β values reported in the table have been used to calculate the charge-state distributions for the RIV nuclei using CHARGE [16]. These distributions are listed in Table II. Since the β values for these systems vary only between 0.060 and 0.061 the charge distributions are very similar and peak near $Q = 31$. The $G_{k,Q}$ values (cf. Eq. (10)) are calculated, as a function of the g factor, as averages over a large number of events. Typically $m = 50,000$ events per charge state are sufficient. The inset of Fig. 2 shows a sample charge-state distribution calculated with $\beta = 0.06$ for the ^{122}Te ions (Table II). The main part of Fig. 2 shows the $G_2(g)$ and $G_4(g)$ functions for a number of the most probable charge states and for the average of all charge states for the ^{122}Te ions. The data points, determined by the g-factor and the G_k values from Ref. [8] (Table I), are also shown in the figure. The effect different charge-state distributions have on the RIV g factors will be discussed in Sec. III C.

At this point, a test of the choice of electronic configurations used in the simulation is in order. Here the crucial input parameter is n_E, used in step (2) of the simulation procedure. Calculations have been performed for configurations with $n_E = 1, 2$ and 3 in the valence shell. The calculations are compared to the data of Ref. [8]. The comparison is shown in

TABLE I: Conditions and parameters for the RIV experiments in Ref. [6] and G_2 and G_4 values according to Ref. [8].

Isotope	E_{beam}	Target	Thick.	β	E_{recoil}	E_{2^+}	τ_{2^+}	G_2	G_4
	(MeV)		(mg/cm^2)	Rec. ion	(MeV)	(keV)	(ps)		
^{122}Te	366	^{12}C	0.956	0.060	205.45	564.1	10.8(1)	0.358(19)	0.217(11)
^{126}Te	378	"	0.956	0.061	216.63	663.3	6.5(2)	0.506(20)	0.370(12)
^{130}Te	390	"	0.956	0.061	227.83	839.5	3.3(1)	0.628(19)	0.506(12)
^{132}Te	396	"	1.130[a]	0.060	220.45[a]	973.9	2.16(20)[a]	0.701(26)	0.532(17)

[a] Corrected value due to revision in Ref. [14].

TABLE II: Charge-state distributions in (%) for ions of ^{122,126,130,132}Te used in the simulations aimed at determining g factors. The β value used in each case is listed in Table I.

Isotope\Q=	25^+	26^+	27^+	28^+	29^+	30^+	31^+	32^+	33^+	34^+	35^+	36^+
^{122}Te	0.21	0.82	2.55	6.24	11.91	17.68	20.33	18.03	12.28	6.39	2.53	0.76
^{126}Te	0.16	0.66	2.13	5.44	10.84	16.82	20.23	18.78	13.39	7.29	3.02	0.95
^{130}Te	0.13	0.53	1.80	4.76	9.86	15.94	19.99	19.36	14.40	8.18	3.53	1.15
^{132}Te	0.23	0.89	2.74	6.58	12.35	18.00	20.33	17.70	11.84	6.05	2.35	0.69

Fig. 3, using a G_k versus g-factor representation for both the simulation curves and the experimental data.

The $G_k(g)$ curves for $n_E = 2$ (black) are in agreement with the data points, while the $n_E = 1$ and 3 curves are substantially below these points. For the Te isotopes ($\beta = 0.06$), the observation can be explained as following: For the $n_E = 1$ case, the simulation includes a large fraction of the electronic states and correspondingly large hyperfine interaction, and the calculated G_k coefficients are smaller than they should be. For the $n_E = 2$ case, the simulation includes now more electronic states than before and due to the transitions between these states the contributions from all electronic states are properly evaluated. For the $n_E = 3$ case, the simulation again includes a large fraction of electronic states with a larger hyperfine interaction, and the calculated G_k coefficients become smaller again. These remarks come from a close examination of the distributions of the hyperfine interactions for

different n_E values. Further investigations are needed to identify the physics that determines the choice of electronic configurations. Presumably, this choice varies between different regions of the periodic table. For the remaining discussion, only configurations with $n_E = 2$ will be considered when extracting g factors for Te isotopes.

B. Simulations for previously measured g factors for ^{122,126,130,132}Te

Since the hyperfine interaction is essentially independent of the isotope mass, the same electronic configurations ($n_E = 2$) are used in simulations for the four Te isotopes. The G_k curves for the 2_1^+ states of the various Te isotopes are calculated by changing only the value of τ (cf. Table I). Columns two to nine of Table III list the previously reported g factors, the remaining columns the present results.

The simulated G_k versus g-factor curves are plotted in Fig. 4. These are compared with all the g factors from previous measurements [8, 19, 20]. For ^{122}Te, the present simulations agree with all previously reported values within the error bars. For ^{126}Te, however, the previous results are either too small or too large. For ^{130}Te, the simulations agree with the previous reported g factors of Refs. [21–23]. For ^{132}Te, the simulations agree with the g factors of Refs. [19, 20]. By using the G_2 and G_4 values from Ref. [8], the present simulations allow the extraction of new g factors for the 2_1^+ states in ^{122,126,130,132}Te. The final results were obtained as weighted averages of the g factors from G_2 and G_4 (cf. Table III).

TABLE III: The g factors for the first 2^+ states of Te isotopes from previous work and the present analysis.

Isotope	g [21]	g[22]	g[24]	g[23]	g[23]	g[19]	g [8]	g [20]	g this work[a]
^{122}Te	0.33(3)	0.28(5)	0.34(2)	0.33(2)	0.36(2)		0.361(46)		$0.331^{+0.024,\ 0.024}_{-0.026,\ 0.026}$
^{126}Te	0.19(3)		0.34(3)	0.31(4)			0.338(17)		$0.251^{+0.015,\ 0.023}_{-0.012,\ 0.019}$
^{130}Te	0.29(6)	0.33(8)		0.29(5)			0.351(18)		$0.280^{+0.015,\ 0.028}_{-0.011,\ 0.017}$
^{132}Te						0.42(6)[b]	0.46(5)[b]	0.28(15)	$0.359^{+0.024,\ 0.045}_{-0.024,\ 0.041}$
Method	TF	TF	TF	TF	IPAC	RIV	RIV	TF	RIV

[a] The first entries for the uncertainties include only the errors from the G_k values, while the second ones incorporate also those from lifetimes.

[b] Corrected values due to change of the nuclear lifetime [14].

C. Comparisons of various charge-state calculations

The available prescriptions for calculating the charge-state distributions vary somewhat. For comparisons with the charge-state distributions used in this paper, two other types of calculations have been considered, using the Schiwietz and Grande formula [25] (denoted as SG calculations) and the Nikolaev and Dmitriev formula [26] (denoted as ND calculations). These are used hereafter to get charge-state distributions for ^{122,126,130,132}Te respectively. The ND calculations result in almost the same distributions as those in Sec. III A, while the distributions obtained with SG calculations are one unit lower. In Fig. 5 the G_k curves calculated for ^{122}Te with $\beta = 0.06$ are shown. The different charge-state distributions are plotted in the inset. For the four Te isotopes, simulations with SG calculations will result in about 5% differences in g factors, while those with ND calculations result in less than 1% differences. Since both the formula for ND calculations and the arithmetic in CHARGE are based on using carbon targets, the applicability of the charge-state calculation in Sec. III A is justifed.

D. Use of g factor as a function of τ

With the present method a G_k versus g-factor curve is calculated for a fixed value τ. At some future time the nuclear lifetime may be revised, i.e., may have a different value or different uncertainties. Hence it would be helpful to have curves calculated for a set of τ values, which allow recalculation of the g factor. Such curves are provided below. The static model does not have this problem, since G_k values are calculated as functions of the quantity $g\tau$. Nevertheless, when the nuclear-lifetime information changes the results of the static model are subject to re-evaluation as well.

For a set of $G_k(g)$ values from a given experiment the g factors are calculated for a series of τ values. An example for the ^{132}Te case is shown in Fig. 6 where the simulations for G_2 and G_4 are shown as circles and squares, respectively. The calculated values were fitted to the empirical function

$$g(\tau) = a_k \cdot \tau^{b_k}, \text{ for } k = 2, 4. \tag{11}$$

The values are $a_2 = 0.7328$, $b_2 = -0.8994$ and $a_4 = 0.7145$, $b_4 = -0.9068$ for the G_2 and G_4 simulations, respectively. This simple function, which is nearly a hyperbola with $b_k = -1$,

fits the simulations quite well. Note that the $g(\tau)$ curves in Fig. 6 from the G_2 and G_4 measurements are different because they cross the simulated $G_k(g)$ lines at different g values [see Fig. 4(d)]. If the G_k values are remeasured with the same reaction conditions and are found to deviate somewhat from those used in the simulations for the $g(\tau)$ functions, then the $G_k(g)$ curves of Fig. 4(d) can be used to obtain new g values. If the lifetime is found to be different, then the g factor can be corrected incrementally via expression (11) with the a_k and b_k values given above. If a different reaction is used to obtain new G_k values, then new simulations have to be made to provide the appropriate $G_k(g)$ curves. This is because different β values and/or recoil media, such as the target material, need to be considered which give different charge-state distributions.

IV. COMPARISON WITH THEORETICAL MODELS

In this section, the g factors obtained from the present analysis are compared with systematics for g factors of the same states in the neighboring Te isotopes and with predictions from various theoretical models. The measured 2_1^+ g factors for a series of Te isotopes are shown in Fig. 7, together with the g factors for the respective Xe isotones. The low-energy structure of the Te and Xe isotopes under discussion can be characterized as vibrational like, as indicated by level-energy ratios $E(4_1^+)/E(2_1^+) \sim 2$. However, their 2_1^+ g factors indicate a somewhat different trend as a function of N, as suggested by linear fits to the data in Fig. 7. The trend for the Te isotopes is consistent with a sort of Z/A behavior, i.e., it is down-sloping with N. In contrast, the Xe isotopes show an up-sloping trend.

The additional line (dashed-dotted) in Fig. 7(a) represents such Z/A behavior and has been constructed based on the following considerations. Nilsson and Prior [27] showed that the lowering of the g factor from the hydrodynamical, collective Z/A value, seen in several mass regions, is due to a difference in the pairing forces for protons and neutrons. Greiner introduced a transparent procedure for scaling the Z/A value accordingly [28]. We have used the expression in Ref. [28] applicable for vibrational-like nuclei,

$$g = \frac{Z}{A}\left[1 - \frac{4}{3}\frac{N}{A}\left(\sqrt{\frac{G_\pi}{G_\nu}} - 1\right)\right], \tag{12}$$

Here, the pairing-force parameters with the values $G_\pi = 25$ MeV/A and $G_\nu = 18$ MeV/A [27] are used. The resulting function, shown as dashed-dotted line, is sufficiently close to

the data, given that its slope is the important feature. A somewhat lower-lying function for g would be obtained with the set of parameters $G_\pi = 30$ MeV/A, $G_\nu = 20$ MeV/A [29], but the principal observation of a Z/A behavior remains unchanged.

The trend of the 2_1^+ g factors, as a function of N, for the Xe isotopes has been discussed by Otsuka [30], and later by Jakob *et al.* [31], in the framework of the IBM-2 approach of the Interacting Boson Model. For the Xe isotopes under discussion, this approach leads to a parabolic dependence from which the rising branch gives an up-sloping g with increasing N. Even though the present discussion uses the Xe isotopes only to contrast the behavior of the Te isotopes, it is instructive to elaborate on the IBM-2 approach for the g factors [30],

$$g = \frac{N_\pi}{N_\pi + N_\nu} g_\pi^B + \frac{N_\nu}{N_\pi + N_\nu} g_\nu^B, \tag{13}$$

where the number of proton and neutron bosons N_π and N_ν, respectively, are counted from the nearest major shell closure. The g factors of the proton and neutron bosons to first approximation are $g_\pi^B = 1$ and $g_\nu^B = 0$, respectively. They are subject to adjustments that lead then to somewhat smaller values for both bosons. For example, for the Xe isotopes with $N \leq 72$ the original g_π^B value is kept, but $g_\nu^B = -0.1$ [30]. In the Xe region, the term with g_π^B is the leading term. Hence, it seems logical that the Xe isotopes show an IBM-2 like behavior rather than the Te isotopes do, as the former have twice the number of proton bosons ($N_\pi = 2$ versus $N_\pi = 1$).

TABLE IV: Calculated g factors for the first 2^+ states of Te isotopes compared to experimental values obtained from the present analysis.

Isotope	BCS[a]	SMII[b]	QRPA[c]	CD-Bonn[d]	CD-Bonn[e]		NPSM[f]		Experiment[g]
				V_{low-k}	Eff.	Free	$g_{\rm s,eff}$	$g_{\rm s,free}$	this analysis
^{122}Te	0.32								$0.331^{+0.024}_{-0.026}$
^{126}Te	0.26								$0.251^{+0.023}_{-0.019}$
^{130}Te	0.31	0.445			0.341	0.180	0.241	0.188	$0.280^{+0.028}_{-0.017}$
^{132}Te	0.40	0.448	0.491	0.35	0.480	0.288	0.337	0.283	$0.359^{+0.045}_{-0.041}$

[a] Ref. [32], [b] Ref. [31], [c] Ref. [33], [d] Ref. [36], [e]Ref. [34], [f]Ref.[35]

[g] The uncertainties include the errors from the G_k values and the lifetimes.

The 2_1^+ g factors for ^{122,126,130,132}Te have been also subject of theoretical calculations that are not based on an algebraic model. These calculations are summarized in chronological

order in Table IV, and reviewed hereafter. Lombard carried out calculations for low-lying states of even-even nuclei with $90 \leq A \leq 150$ using the pairing-plus-quadrupole model with BCS wavefunctions [32]. The results for the relevant Te isotopes are listed in the column labeled BCS. The already cited paper by Jakob *et al.* also contains shell-model calculations for ^{130,132}Te [31]. These authors use surface-delta interactions, to describe the two-body residual interactions. Their results are listed in the column labeled SMII. Terasaki et al. [33] used a separable quadrupole-plus-pairing Hamiltonian and the quasiparticle random phase approximation to calculate g factors for the lowest 2^+ states near ^{132}Sn. The result for ^{132}Te is shown in column labeled QRPA. Brown *et al.* did shell-model calculations of g factors for Sn to Xe nuclei, including ^{130,132}Te [34]. The authors used a residual interaction based on the CD-Bonn nucleon-nucleon interaction. They determine the single-particle spin and orbital effective g factors by including both core-polarization and meson-exchange current effects. Two different g factors are given, one obtained with an effective and one with a free-nucleon magnetic-moment operator. These are listed in a group of two columns, labeled CD-Bonn-Eff and CD-Bonn-Free. Jia *et al.* carried out calculations for low-energy spectra of even-even nuclei, including ^{130,132}Te, with the so-called nucleon-pair approximation of the shell model [35]. They performed two sets of calculations, one with the free-nucleon spin g factor, g_s, the other one with a quenched g_s value assuming a reduction factor of 0.7. Their results are listed in a group of two columns, labeled NPSM-$g_{\rm s,eff}$ and NPSM-$g_{\rm s,free}$, which correspond to the "quenched" and free-nucleon cases, respectively. A recent calculation of the 2_1^+ g factor for ^{132}Te using the Monte-Carlo shell-model approach is communicated in the literature [20]. In this calculation, g_s is assumed to be quenched by 0.7, and a value $g = 0.29$ is obtained.

The calculations of Ref. [32] agree overall with the present experimental results. The overestimation of the 2_1^+ g factors for ^{130,132}Te in Ref. [31] has been attributed to the strength of the proton-neutron interactions, which is adjustable. Neither the QRPA calculations nor the CD-Bonn-Free and the CD-Bonn-Eff calculations agree with the present results. However, the approach of Ref. [36] using CD-Bonn potential through the so-called low momentum V_{low-k} approach labeled as CD-Bonn_V_{low-k} agrees with present result for ^{132}Te. The comparison also shows preference for the NPSM $g_{s,eff}$ calculations of Ref. [35].

V. SUMMARY AND CONCLUSIONS

In summary, the present method of calculating attenuation coefficients G_k of γ-ray angular distributions or particle-γ angular correlations is a time-dependent simulation where the nuclear and atomic lifetimes are compared on an event-by-event basis and many atomic states are sampled by random-number choices for each event (Monte-Carlo simulations). A crucial input to the simulations is obtained from atomic-structure calculations with the code GRASP2K. The simulation results are compared with previously reported g factors measured with the RIV and TF techniques. Agreement is found with most of the previously reported g factors of the 2_1^+ states of ^{122,130,132}Te. The simulated result for the 2_1^+ state of ^{126}Te does not agree with any of the reported values. On the other hand, this particular data point lies systematically lower in several data sets including the present one and the one of Ref. [21]. There is a similar trend between the g factors for ^{122,126,130,132}Te in present analysis and the values from Ref. [17], but the differences for ^{126,130,132}Te are outside the quoted uncertainties. The g factors obtained from the present simulations are also compared with theoretical models, and some level of agreement is found. However, there is room for improvement in the theoretical calculations.

Unlike the previously used methods to analyze the RIV measurements, the present simulation method is essentially parameter free. Once the electronic configurations are chosen, they don't need to be changed when the nuclear lifetime varies (or a different nuclear spin state is considered).

The Te isotopes under discussion have been produced via inverse-kinematic Coulomb excitation at recoil velocities of $\beta = 0.06$. Future experiments with radioactive-ion beams similar to the RIV ^{132}Te experiment are conceivable. If performed near the Coulomb barrier, β values in the range 0.05 - 0.07 can be obtained, suggesting the use of the present type of analysis in order to extract RIV g factors.

Acknowledgments

One of the authors (X. C.) thanks N. J. Stone (Oxford) and J. R. Stone (Oxford) for valuable discussions and assistance during the early phase of this work especially in the use of the GRASP2K code and L. Qin (Hewlett-Packard) for helping with the installation of the

code GRASP2K. Many informative discussions with A. E. Stuchbery (Australian National University) are acknowledged; he has pointed out to us that the formulas used in Sec. III C should be considered. This work was supported by the US Department of Energy, Office of Nuclear Physics, grant no. DE-FG02-88ER-40406.

---

[1] G. Goldring, *Hyperfine interactions in isolated ions* (North-Holland, Amsterdam, 1982), Vol. **5**, p. 484.

[2] G. Goldring, D. A. Hutcheon, W. L. Randolph, D. F. H. Start, M. B. Goldberg, and M. Popp, Phys. Rev. Lett. **28**, 763 (1972).

[3] C. Broude, M. B. Goldberg, G. Goldring, M. Hass, M. J. Renan, B. Sharon, Z. Shkedi, and D. F. H. Start, Nucl. Phys. **A 215**, 617 (1973).

[4] R. E. Horstman, J. L. Eberhardt, H. A. Doubt, C. M. E. Otten, and G. Van Middelkoop, Nucl. Phys. **A 248**, 291 (1975).

[5] D. Ward, H. R. Andrews, R. L. Graham, J. S. Geiger, and N. Rud, Nucl. Phys. **A 234**, 94 (1974).

[6] N. J. Stone, A. E. Stuchbery, M. Danchev, J. Pavan, C. L. Timlin, C. Baktash, C. Barton, J. Beene, N. Benczer-Koller, C. R. Bingham *et al.*, Phys. Rev. Lett. **94**, 192501 (2005).

[7] N. Benczer-Koller and G. J. Kumbartzki, Journal of Physics G: Nuclear and Particle Physics **34**, R321 (2007), and references therein.

[8] A. E. Stuchbery and N. J. Stone, Phys. Rev. C **76**, 034307 (2007).

[9] D. Radeck, V. Werner, G. Ilie, N. Cooper, V. Anagnostatou, T. Ahn, L. Bettermann, R. J. Casperson, R. Chevrier, A. Heinz *et al.*, Phys. Rev. C **85**, 014301 (2012).

[10] C. F. Fischer, T. Brage, and P. Jönsson, Computational Atomic Structure, An MCHF Approach (Institute of Physics Publishing, 1997).

[11] N. Stone, J. Stone, and P. Jönsson, Hyperfine Interact. **197**, 29 (2010).

[12] C. Froese Fischer, G. Tachiev, and A. Irimia, At. Data Nucl. Data Tables **92**, 607 (2006).

[13] D. C. Radford, C. Baktash, J. R. Beene, B. Fuentes, A. Galindo-Uribarri, C. J. Gross, P. A. Hausladen, T. A. Lewis, P. E. Mueller, E. Padilla *et al.*, Phys. Rev. Lett. **88**, 222501 (2002).

[14] M. Danchev, G. Rainovski, N. Pietralla, A. Gargano, A. Covello, C. Baktash, J. R. Beene, C. R. Bingham, A. Galindo-Uribarri, K. A. Gladnishki *et al.*, Phys. Rev. **C 84**, 061306 (2011).

[15] P. Jönsson, X. He, C. Froese Fischer, and I. P. Grant, Computer Physics Communications **177**, 597 (2007).

[16] Code CHARGE by R. O. Sayer, Internal Lab Memo, Oak Ridge National Lab, 1978.

[17] A. E. Stuchbery, A. Nakamura, A. N. Wilson, P. M. Davidson, H. Watanabe, and A. I. Levon, Phys. Rev. **C 76**, 034306 (2007).

[18] S. Raman, C. W. Nestor Jr., and P. Tikkanen, At. Data Nucl. Data Tables **78**, 1 (2001).

[19] N. J. Stone, At. Data Nucl. Data Tables **90**, 75 (2005).

[20] N. Benczer-Koller, *et al.*, Phys. Lett. B **664**, 241 (2008).

[21] N. K. B. Shu, R. Levy, N. Tsoupas, A. Lopez-Garcia, W. Andrejtscheff, and N. Benczer-Koller, Phys. Rev. **C 2**4, 954 (1981).

[22] A. P. Grinberg, M. F. Kudoyarov, A. A. Pasternak, and L. A. Rassadin, Bulletin of the Academy of Sciences of the USSR, Physical Series **49**, 2137 (1985).

[23] J. S. Dunham, R. T. Westervelt, R. Avida, and S. S. Hanna, Phys. Rev. **C 37**, 2881 (1988).

[24] J. L. Thornton, B. T. Neyer, and S. S. Hanna, Bull. Am. Phys. Soc. **30**, 1284 (1985).

[25] G. Shiwietz,and P. L. Grande, Nucl. Instrum. Meth. in Phys. Research B **175-177,** 125 (2001).

[26] V. S. Nikolaev, and I. S. Dmitriev, Phys. Lett. A**28**, 277(1968).

[27] S. G. Nilsson and O. Prior, Mat. Phys. Medd. Dan. Vid. Selsk. **32**, No. 16 (1961).

[28] W. Greiner, Nucl. Phys. **80**, 417 (1966).

[29] E. R. Marschalek and J. O. Rasmussen, Nucl. Phys. A **43**, 438 (1963).

[30] T. Otsuka, Hyperfine Interactions **78** (1993) 19.

[31] G. Jakob, *et al.*, Phys. Rev. C **65**, 024316 (2002).

[32] R. J. Lombard, Nucl. Phys. A **114**, 449 (1968).

[33] J. Terasaki, J. Engel, W. Nazarewicz, and M. Stoitsov, Phys. Rev. **C 66**, 054313 (2002).

[34] B. A. Brown, N. J. Stone, J. R. Stone, I. S. Towner, and M. Hjorth-Jensen, Phys. Rev. **C 71**, 044317 (2005).

[35] L. Y. Jia, H. Zhang, and Y. M. Zhao, Phys. Rev. C **75**, 034307 (2007).

[36] L. Coraggio, A. Covello, A. Gargano, N. Itaco, and T.Kuo, Phys. Rev. C**66**, 064311 (2002).

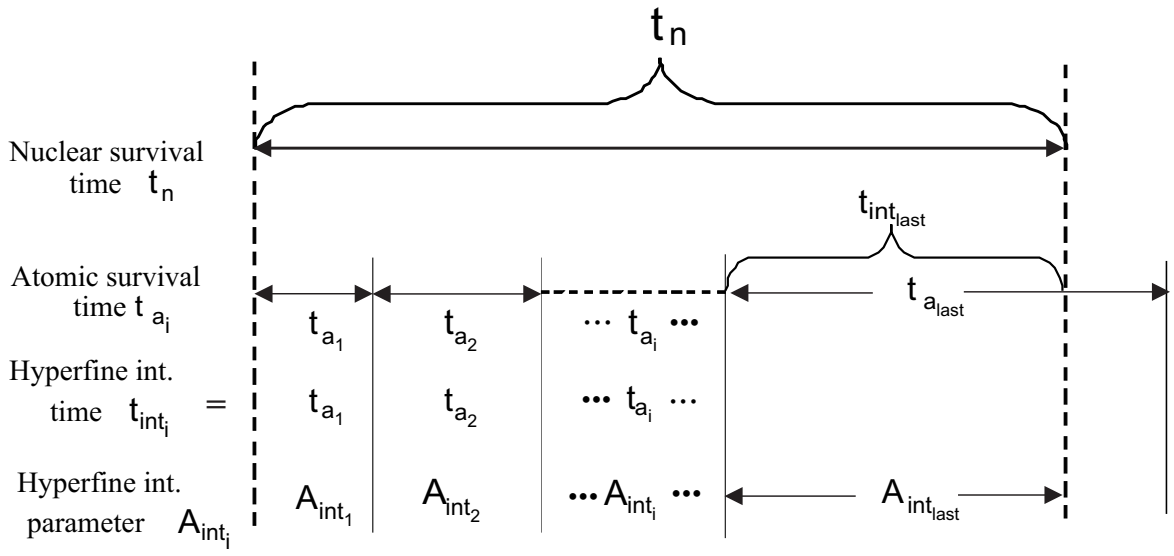

FIG. 1: The concept for the Monte-Carlo simulations in the present work. The time sequence for successive atomic transitions are indicated. The last transition has a time $t_{a,last}$ that exceeds the nuclear time t_n and that terminates the event. The equations for the calculations are given in the text.

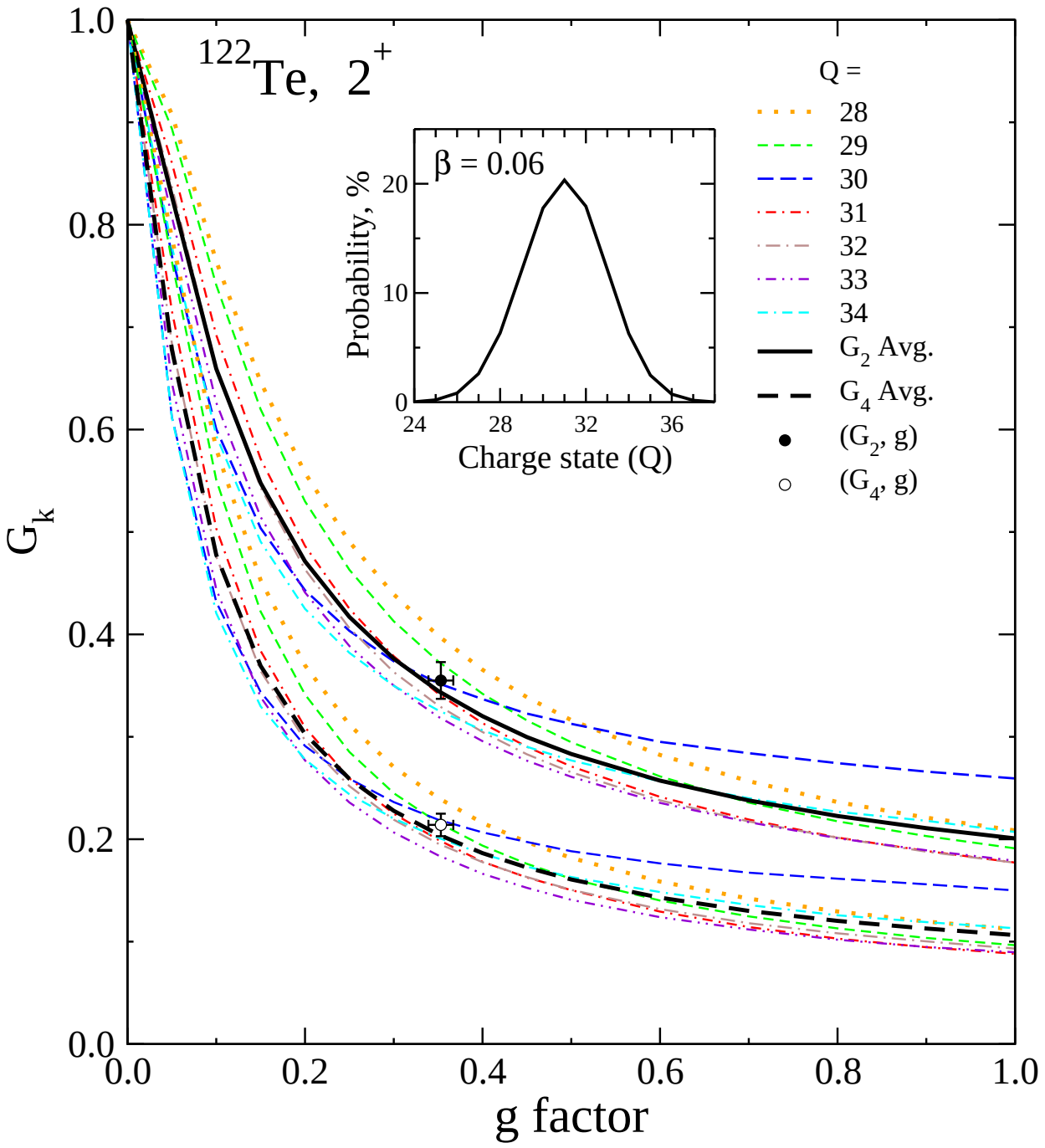

FIG. 2: The averaged G_k versus g-factor curves (thick black lines) for 2_1^+ state of ^{122}Te over all charge states after recoiling into vacuum and the contributions of G_k (thin dashed lines) from individual charge states. The data points are from Ref. [8]. The inset shows the charge-state distribution calculated for an ion velocity β= 0.06 (see text). (Color online).

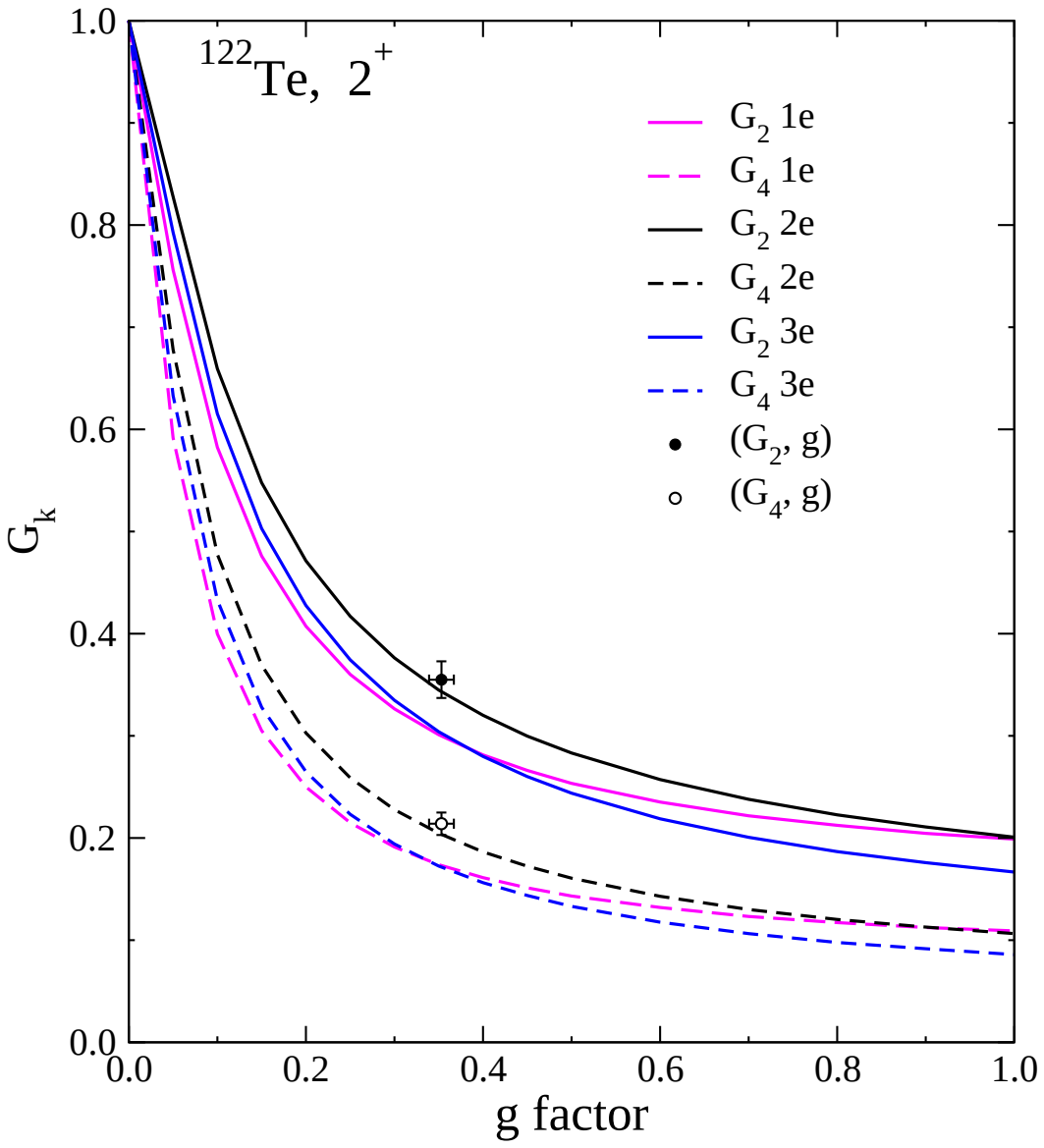

FIG. 3: Comparisons of RIV data for ^{122}Te [8] with G_k versus g- factor curves simulated with the number of electron excitations n_E =1,2 and 3. (Color online).

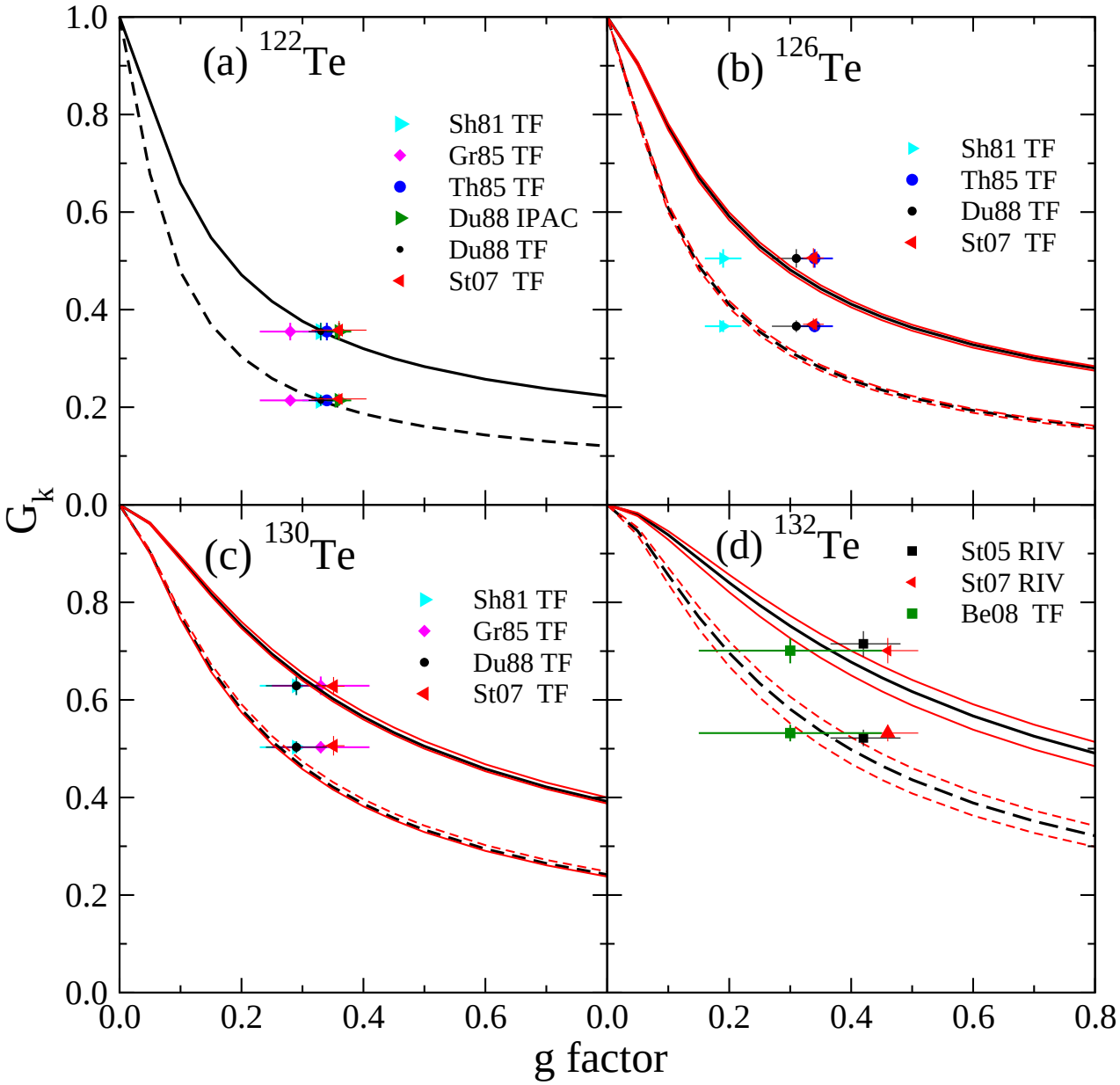

FIG. 4: Calculated curves of G_2 (solid curves) and G_4 (dashed curves) as functions of the g factor for ^{122,126,130,132}Te. They are compared with previously reported g factors from different measurements, mainly transient field method. The previously measured g factors are labeled as "Sh81 TF" [21], "Gr85 TF" [22], "Th85 TF" [24], "Du88 IPAC" [23], "Du88 TF" [23], "St07 TF" [17], "St07 RIV" [8], "St05 RIV" [19] and "Be08 TF" [20]. In panels (b), (c), and (d), the family of curves for a certain G_k represents the average value (black) and the uncertainties in τ (red). The uncertainties of G_k curves in panel (a) are very small due to small uncertainty of τ and thus is not shown in the figure. (Color online)

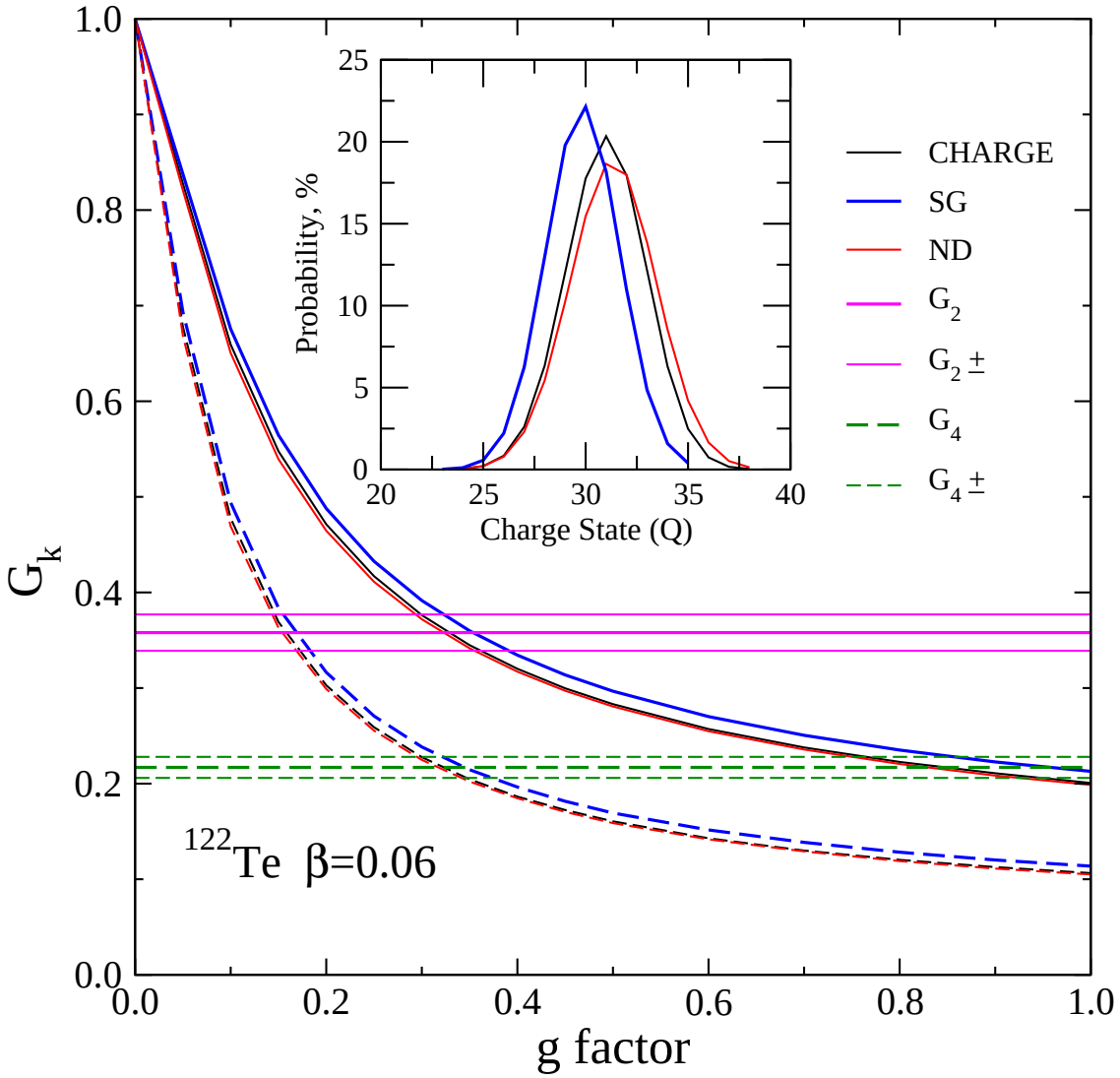

FIG. 5: Comparisons of G_k versus g-factor curves obtained for ^{122}Te with different charge-state distributions calculated with CHARGE (this work), and the SG and ND formulae. The sets of horizontal solid and dashed lines indicate the reported G_2 and G_4 values (including errors), respectively [8]. (Color online)

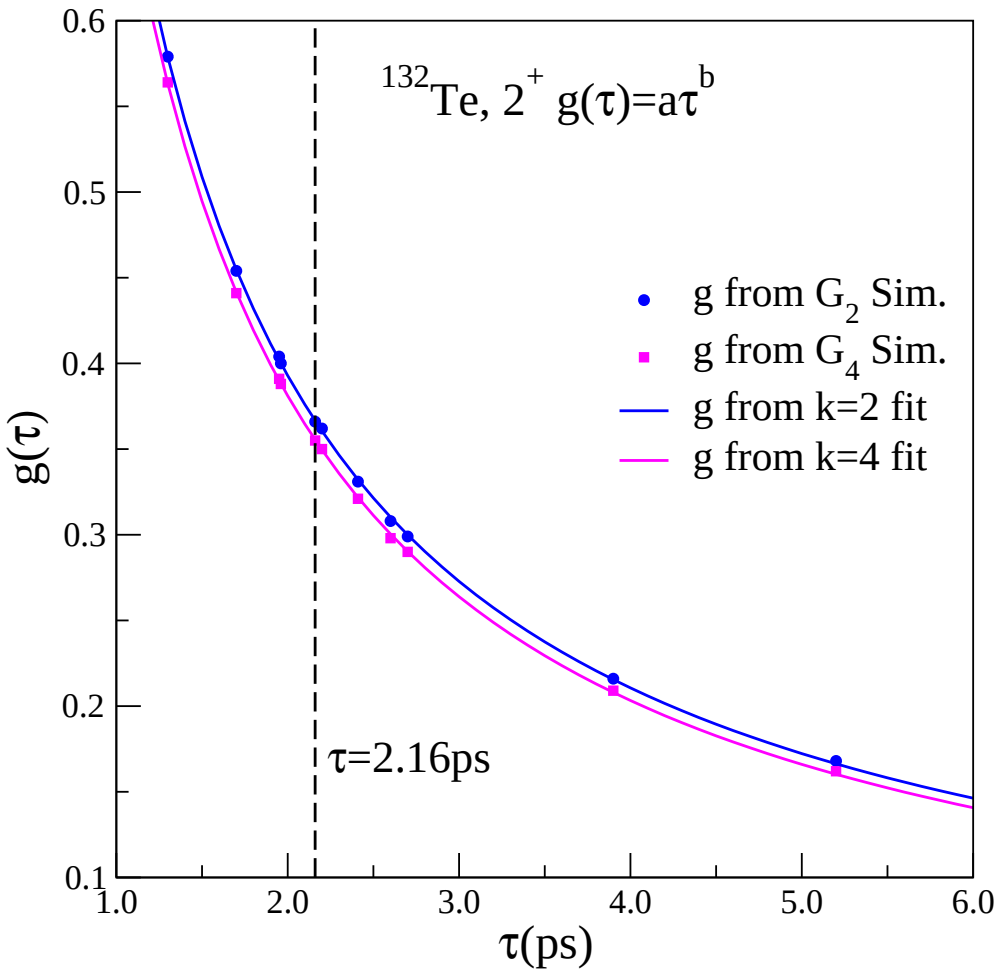

FIG. 6: Interpolated g factor for ^{132}Te for different values of τ around the present value of 2.16 ps, which is indicated by the vertical dashed line. (Color online)

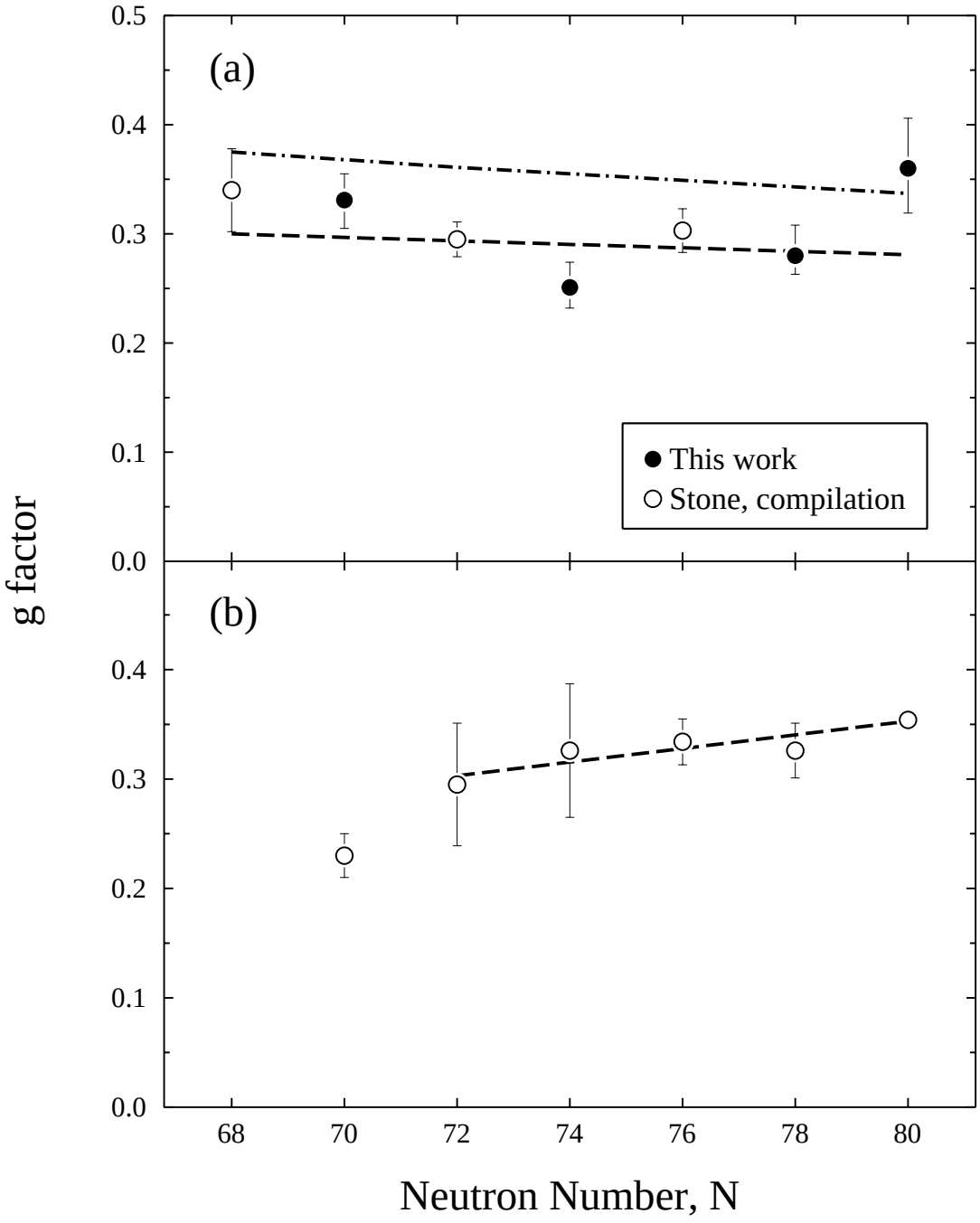

FIG. 7: The g factors for the 2_1^+ states in a series of (a) Te and (b) Xe isotopes. The values obtained from the present RIV analysis and values determined as weighted averages from the compilation of Ref. [19] are distinguished by filled and open symbols, respectively. The dashed lines represent linear fits to the data. The dash-dotted line in panel (a) is a "scaled" Z/A function (see text). The uncertainty of the point at $N = 80$ on panel (b) is smaller than the symbol.